Contents list available at CBIORE journal website

International Journal of Renewable Energy Development

Journal homepage: https://ijred.cbiore.id

Research Article

Numerical and experimental investigations on a bladeless turbine: Tesla's cohesion-type innovation

Malayathi Sivaramakrishnaiah[1,*], Dhanaraj Savary Nasan[2], Prabhakar Sharma[3], Thanh Tuan Le[4], Minh Ho Tran[5,*], Thi Bich Ngoc Nguyen[6], Phuoc Quy Phong Nguyen[7], Viet Dung Tran[7,*]

[1]*Department of Mechanical Engineering, SVR Engineering College, Nandyal, Kurnool, Andhra Pradesh-518502, India.*

[2]*Department of Mechanical Engineering, St.Martin's Engineering College, Secunderabad- 500100, TS, India.*

[3]*Department of Mechanical Engineering, Delhi Skill and Entrepreneurship University, Delhi, India.*

[4]*Institute of Engineering, HUTECH University, Ho Chi Minh City, Viet Nam.*

[5]*Faculty of Automotive Engineering, Dong A University, Danang, Viet Nam.*

[6]*Faculty of Electrical and Electronics Engineering, Ho Chi Minh City University of Transport, Ho Chi Minh City, Viet Nam.*

[7]*PATET Research Group, Ho Chi Minh City University of Transport, Ho Chi Minh City, Viet Nam*

Abstract. The design, numerical simulation, manufacturing, and physical experimentation of Tesla's bladeless centripetal turbine for electrical power production are the topics of this research project. The turbine generates rotational motion in the discs by directing pressurized air and water tangentially across parallel smooth disc surfaces. The fluid speed parameter at the nozzle inlet determines the power generated. To ensure optimal mechanical design parameters, SolidWorks design software, fluid dynamics concepts, and machine element design were employed. The numerical simulation software ANSYS CFX was used. The numerical and qualitative findings of the models and physical experiments coincided well. The study revealed that the power production and turbine efficiency were regulated by the input sources and blade size. Variations in the fluid composition between the discs may additionally have an impact on the outcomes. The researchers investigated the connection between input fluid pressure and turbine efficiency, as well as the number of discs and turbine power. The prototype could generate 76.52 W of electricity at 50 bar pressure and 1.01e+05 Reynolds number. The operation was efficiently simulated using CFD, with only a 9.3% difference between experimental and simulated results. Overall, this research provides an in-depth assessment of Tesla's bladeless centripetal turbine. It verifies the design and numerical simulation methodologies used, as well as identifies the essential aspects impacting turbine performance and efficiency. The findings contribute to a better understanding of the turbine's behavior and give ideas for improving its performance.

Keywords: Tesla turbine; Cohesion type bladeless turbine; Tangential fluid flow; Viscous and adhesive forces; Plenum chamber; Pico hydro systems.

Received: 15th May 2023; Revised: 25th Oct 2023; Accepted: 26th Nov 2023; Available online: 7th Dec 2023

1. Introduction

Wind is one of renewable energy forms that has been paid attention to recently because it is considered as clean and green energy with non-carbon emissions (Marih *et al*., 2020)(Nguyen *et al*., 2021)(Hassoine *et al*., 2022). Thus, studies on wind turbine are taken the great interest (Sang *et al*., 2017) Shoukat *et al*., 2021). In contrast to conventional turbines that depended on fluid impinging on curved blades, Nikola Tesla revolutionized the field by exploiting the boundary layer effect of fluid on flat, circular discs to generate mechanical rotary power (Talluri *et al*., 2018). Tesla was given a patent for his innovative concept and mechanism, which became known as the Tesla Turbine, his patent emphasized the significance of gradual changes in fluid speed and direction to maximize turbomachine efficiency (Manfrida *et al*., 2018). Due to this slow energy transfer method, Tesla claimed a phenomenal efficiency of approximately 95%. An extensive study was conducted, inspired by Tesla's physics, to build Tesla turbines that offered optimal performance and economic viability (Qi *et al*., 2019). This section looks into Tesla's initial design, following contributions by numerous researchers, and the underlying theory. Leeman (Leaman, 1950) built a turbine with a central exhaust using 126 mm diameter discs and with a maximum inlet pressure of 85 psi. The maximum speed reached was over 9,000 rpm, with an efficiency of 8.24%. The researchers investigated the effects based on several surface textures of discs and reported that smooth discs perform marginally superior than rough discs. The turbine had 126 mm diameter discs with a maximum inlet pressure of 85 psi. It reached speeds of more than 9,000 rpm while maintaining an efficiency of 8.24%. Leeman's design diverged slightly from Tesla's original proposal, featuring a central cavity for exhaust delivery and a slotted shaft to facilitate exhaust flow. He also investigated the effect of different surface textures on disc performance, determining that smooth discs had a modest edge over rough discs. This study is an important step forward in turbine development since it demonstrated Tesla's visionary

* Corresponding author
Email : scopusscimsk@gmail.com (M. Sivaramakrishnaiah); hotm@donga.edu.vn (M. H. Tran); dungtv@ut.edu.vn (V. D. Tran)

https://doi.org/10.14710/ijred.2024.55455
ISSN: 2252-4940/© 2024.The Author(s). Published by CBIORE

boundary layer notion and subsequent advances by researchers. The use of flat discs instead of standard blades brings up new opportunities for improving turbine efficiency and performance. These studies' findings establish the groundwork for additional investigation and breakthroughs in Tesla turbine design, with the potential to revolutionize the area of fluid engineering (Alanne and Cao, 2019; Alonso and Silva, 2022).

Talluri *et al*. (Talluri *et al*., 2018) investigated Tesla turbine architecture for Organic Rankine Cycle (ORC) usage in small-micro power generation. The Tesla turbine, a bladeless viscous turbine concept proposed by Nikola Tesla, has resurfaced due to its suitability for low-cost components in small-scale systems such as ORC. The study used an optimization method and a novel rotor model to evaluate three turbine layouts of varying sizes. With N-hexane fluid, the Tesla turbine obtained a total-to-static efficiency of 64%. Talluri *et al*. (Talluri *et al*., 2020) examined the efficiency and dependability of the Tesla turbine in miniature power generation with ORC. They evaluated the turbine functioning with R1233zd(E) experimentally, accounting for the blockage effect generated by disc edges, which resulted in flow deviation and performance losses. With a peak net power output of 371 W, a peak shaft efficiency of 9.62%, and a maximum adiabatic efficiency of 30%, the results proved the possibility of using Tesla turbines in ORC applications. The findings help to better understand and enhance turbine design for ORC, especially in the setting of micro power generation that has low inlet temperature and expansion ratios. Huynh *et al*. (Huynh *et al*., 2021) examined the efficacy of a hybrid energy harvesting system that integrated a Tesla turbine design, triboelectric nanogenerators (TENGs), and an electromagnetic generator (EMG). TENG-EMG (T3-E) optimized Tesla turbine displayed high output voltage-current and prolonged running time. TENG and EMG achieved peak outputs of 312.5 V/82 A and 4.2 V/3.3 mA, correspondingly, with operation durations of 20 s and 38 s. Having outputs of 332 V/3.5 mA and operation times of 20 s for voltage and 40 s for current, the hybrid system considerably improved performance. These findings meet the energy requirements of portable electric loads, and practical uses such as LED lighting and IoT wireless sensor operation have been proven. This hybrid generator idea has a lot of possibilities for capturing biomechanical energy. Another study by Ciappi *et al*. (Ciappi *et al*., 2019) investigated the efficiency prediction and flow properties of a Tesla turbine working with organic fluids using a 2D in-house code and computational fluid dynamics (CFD) modeling in another study. Various working fluids (R404a, R134a, and R245fa) were studied, and a small-scale prototype demonstrated good rotor efficiency (69% at 3000 rpm). The CFD calculations and in-house code agreed perfectly. Furthermore, fluid dynamics within the channel have been studied using absolute and relative flow route lines, revealing fundamental flow phenomena. This analysis and comparison will help to gain a greater understanding of the Tesla turbine's performance in low-power applications with various organic fluids.

In medium-head conditions, the turbine's greater working speed makes it more practical to link the turbine shaft directly to the generator, removing the requirement for a gearbox system (Pandey *et al*., 2014)(Dzida *et al*., 2009)(Świrydczuk, 2013). It was found that the rectangular nozzle shape advantageously enables flow contact with the whole set of discs. The rectangular nozzle design advantageously provides flow contact with the full set of discs, which occurs at different places during entry and departure from the casing (Galindo *et al*., 2021). For a basic design, efficiencies can vary from 65% to 80%, while more complicated systems can achieve efficiencies of up to 85%. Peirs *et al*. (Peirs *et al*., 2003) concentrated on a 10 mm diameter rotor disc turbine, signifying an important milestone in the creation of a micro-generator that uses fuel to generate electricity. This turbine reached a power output of 28 W with an efficiency of 18% while operating at an amazing speed of 160,000 rpm. Herrault *et al*. (Herrault *et al*., 2010) employed the silicon-packed permanent magnet micro-generators. The advantage of silicon packaging is the fine control of shape and dimensions during batch production. This has resulted in high speed and hence ultimate compactness of the device. The research on the Tesla turbine was enriched by several researchers in the recent past (Qi *et al*., 2023; Rusin *et al*., 2019; Song *et al*., 2018, 2017; Zuber *et al*., 2019). Deam *et al*. (Deam *et al*., 2008) proved that small-scale viscous turbines outperform conventional bladed turbines. Hoya and Guha (Hoya and Guha, 2009) employed a novel design with slight adjustments around the input nozzle. The turbine efficiency grew with angular speed until it reached a maximum pressure of 140W. At this stage, accounting for frictional torque inside the system, they reached a 25% efficiency at an input pressure of 3.8 bar. Their investigation revealed the possibility of increasing efficiency by minimizing nozzle losses. Guha and Smiley (Guha and Smiley, 2010) replaced the standard nozzle-inlet assembly with a redesigned plenum chamber input nozzle, which resulted in better turbine performance by a 40-50 reduction in total pressure loss and improved jet uniformity, resulting in uniform inlet conditions for all discs passes. Furthermore, Tesla turbines are appropriate expanders for the ORC. Ho-Yan (Ho-Yan, 2011) reported that Tesla turbine designs are better suited for high-head applications but provide poor power densities based on Rice's idealized model. These research efforts contribute to the continued investigation and optimization of Tesla turbine designs, providing insights into improving efficiency, lowering losses, and broadening their use in other energy systems. Sengupta *et al*. (Sengupta and Guha, 2016) employed nano-fluid for the Tesla turbine's 100m distant discs, namely a dilute solution of Ferro-particles in water. Their research found that raising the volume percentage of nanoparticles from 0.00 to 0.05 might result in a 30% increase in power output. Rusin *et al*. (Rusin *et al*., 2018) used the ANSYS CFX 18 commercial code to simulate a 73mm Tesla turbine with three distinct turbulence models: RNG k-ε, k-ω SST, and SAS. Using a denser mesh and a lower temporal step for the SAS turbulence model allowed for greater analysis of minor vortex components and unsteadiness. When compared to the RNG k- and k- SST turbulence models, the exact mesh produced the maximum unit power. Zuber *et al*. (Zuber *et al*., 2019) identified two major constraints influencing Tesla turbine efficiency. For starters, the inefficiency of the nozzle design has a substantial influence on total efficiency, necessitating more concentrated research in this area. Second, while high disc spinning speeds improve turbine efficiency, they offer issues in terms of disc warping at such RPMs. One proposed option is to use high-priced advanced raw material sheets for the turbine discs, albeit this will increase the equipment cost. These novel ideas in Tesla turbine research provide new opportunities for improving performance and tackling efficiency challenges. Additional research and optimizations in nozzle design and material choices have the potential to significantly enhance total turbine efficiency.

The purpose of this study work is to fill many gaps in the literature while contributing to the discipline of turbine design and performance. The relevance of material selection for turbine primary parts, such as the casing, inlet nozzle, annular discs, and shaft, is one significant element investigated in this paper. The relationship that exists between the turbine's intake and output characteristics is explored using computational and experimental investigations, with a focus on the connection

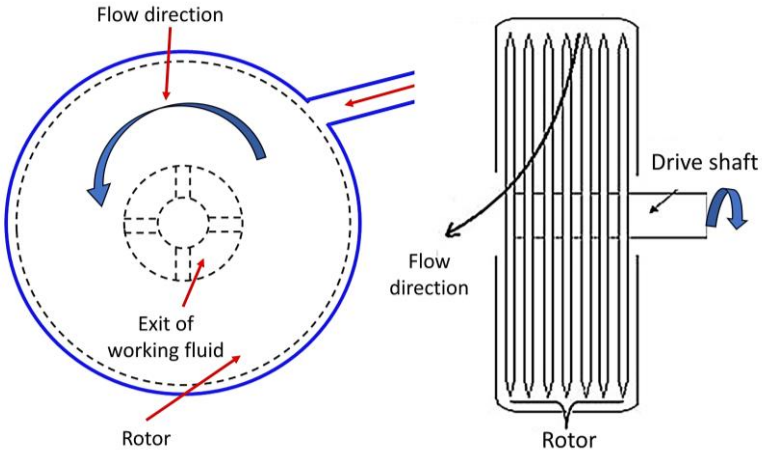

Fig 1. Tesla turbine flow domain

between inlet fluid pressure and turbine efficiency, and also the effect of the number of discs on turbine power. Another noteworthy part of the research is the investigation of the effect of input size and blade size on power generation and machine efficiency. This research provides important insights into the best design choices for turbine components. To analyze and enhance turbine performance, the study employs traditional design approaches such as SolidWorks and fluid mechanics theory, as well as CFD simulations and practical experimentation. The application of CFD simulation findings to improve turbine efficiency through design changes is a notable novelty in this work. The study investigates possible enhancements in turbine performance based on CFD calculations and then validates these gains with rig tests of the revised components using a prototype Tesla turbine. In addition, the study emphasizes the use of air that is compressed as the working fluid, paving the path for further research into the implementation of the prototype Tesla turbine in harvesting wind energy for the generation of electricity.

2. Methodology

2.1 Design principal and consideration

The design ideas and concerns for the bladeless turbine based on Tesla's cohesion-type invention are given in this section. The impinging action of fluid, slow energy transfer, and the requirement for changes in fluid speed and direction are all discussed (Ernnie Illyani Basri *et al*., 2023). The design concepts form the basis for creating an efficient and effective turbine system. Based on a detailed literature survey (Aghagoli and Sorin, 2020; Ciappi *et al*., 2019; Manfrida and Talluri, 2019; Renuke *et al*., 2019), it was evidenced, that the overall efficiency of the Tesla turbine lies in the range of 6-12%. Further based on different parameters study, it was noticed that the power output and hence the overall efficiency is affected by the variation in some parameters. Based on a non-conventional concept which is a bladeless turbomachine, the Tesla turbine is not yet developed for any commercial application. Since the turbine‘s efficiency is very much less; it is not yet developed to its full extent. In the present work, a prototype of a Tesla turbine is built with increased efficiency by increasing the number of roto discs. Further, the turbine's performance is studied under various test conditions, and potential applications of this bladeless turbomachine are explored (Ciappi *et al*., 2019)(Placco and Guimarães, 2020)(Ferrando *et al*., 2021).

Based on the physics of fluid dynamics, theoretical calculations, and Solid Works software, mechanical design and drawings of relevant components of the turbine were carried out as per flow domain **Figure 1**. With the initial availability of modeling of the turbine as input, CFD simulation is carried out by ANSYS software to improve the turbine's output performance. The CFD process for the present work can be described assuming the model's major characteristics being the assumptions of genuine compressible fluid characteristics and constant viscous and laminar flow. The equations for Navier-Stokes in cylindrical coordinates can be reduced using these assumptions (Eq. (1) to Eq. (5)). In comparison, body forces were considered to be insignificant to viscous flow:

$$(1/r) * \partial(ru_r)/\partial r + (1/r) * \partial u_\theta/\partial\theta + \partial u_z/\partial z = 0 \quad (1)$$

The equations for momentum:

$$\partial u_r/\partial t + (u_r * \partial u_r/\partial r + (u_\theta/r) * \partial u_r/\partial\theta + (u_z/r) * \partial u_r/\partial z = -(1/\rho) * \partial p/\partial r + (\nu/r\hat{}2) * (\partial/\partial r)(r\hat{}2 * \partial u_r/\partial r) + (\nu/r\hat{}2) * (\partial\hat{}2u_r/\partial\theta\hat{}2) + (\partial\hat{}2u_r/\partial z\hat{}2) \quad (2)$$

$$(1/r) * \partial u_\theta/\partial t + (u_r * \partial u_\theta/\partial r + (u_\theta/r) * \partial u_\theta/\partial\theta + (u_z/r) * \partial u_\theta/\partial z = -(1/\rho) * (1/r) * \partial p/\partial\theta + (\nu/r\hat{}2) * (\partial/\partial r)(r\hat{}2 * \partial u_\theta/\partial r) + (\nu/r\hat{}2) * (\partial\hat{}2u_\theta/\partial\theta\hat{}2) + (\partial\hat{}2u_\theta/\partial z\hat{}2) - (u_r\hat{}2/r) \quad (3)$$

$$\partial u_z/\partial t + (u_r * \partial u_z/\partial r + (u_\theta/r) * \partial u_z/\partial\theta + (u_z/r) * \partial u_z/\partial z = -(1/\rho) * \partial p/\partial z + (\nu/r\hat{}2) * (\partial/\partial r)(r\hat{}2 * \partial u_z/\partial r) + (\nu/r\hat{}2) * (\partial\hat{}2u_z/\partial\theta\hat{}2) + (\partial\hat{}2u_z/\partial z\hat{}2) \quad (4)$$

The equations for energy are:

$$\partial T/\partial t + (u_r * \partial T/\partial r + (u_\theta/r) * \partial T/\partial\theta + u_z * \partial T/\partial z = \alpha * [(1/r) * \partial/\partial r\,(r * \partial T/\partial r) + (1/r\hat{}2) * \partial\hat{}2T/\partial\theta\hat{}2 + \partial\hat{}2T/\partial z\hat{}2] + Q \quad (5)$$

.

Based on the simulation results, mechanical design specifications are modified and finalized (Thomazoni *et al*., 2022)(Mohammadpour *et al*., 2021)(Arun *et al*., 2021). Continuing the simulation, boundary conditions were applied for finalized design to evaluate various parameters in conformance with the design (Yogesh Babu *et al*., 2020). The

Table 1
Particulars of 7075 Aluminium alloy, 316 Stainless Steel and EN 24 Steel

Particulars	7075 Aluminium Alloy	316 Stainless Steel	EN 24 Steel
Compositions	90% Al, 5.6–6.1% Zn, 2.1–2.5% Mg, 1.2–1.6% Cu, and less than 0.5% of Si, Fe, Mn, Ti, Cr, and other metals	16.0-18.0%Cr, 10.0-14.0% Ni, 2.00 -3.00 % Mo, 0.00-0.045% P, max 0.08% C, max 2.0 % Mn, max 0.75% Si, max 0.03 % S, and max 0.10 % N	0.36-0.44% of C, 0.1-0.35% Si, 0.45-0.7% Mn, 1-1.4% Cr, 0.2-0.35% Mo, 1.3-1.7% Ni, max 0.04% S, and max 0.035% P
Density (kg/m^3)	2810	8000	7850
Young's modulus (GPa)	75	193	120
Thermal conductivity, (W/mK)	23.2	16.3	32
Tensile strength (N/mm^2)	276	515	680

turbine output is computed as per the design requirements. A comparison study of theoretical, physical, and numerical experimental values was carried out to evaluate the percentage error as per the selected parameters. The sequential steps adopted in the present work; mechanical design of parts by theoretical calculations and Solid software, material selection for each part, procurement of readily available parts, manufacturing and fabrication processes, assembly of parts, testing of the turbine, CFD simulations of blades and nozzles in ANSYS 18.0, data collection and analysis, calculations, results and discussions, and conclusion..

2.2 Material selection

The casing and intake nozzle of the bladeless turbine was made out of 7075 Al, an aerospace-grade Aluminum alloy. This alloy has a high strength-to-weight ratio and outstanding strength similar to many sheets of steel, making it perfect for aeronautical applications (LI *et al*., 2023; Mandaloi *et al*., 2022). It also has high fatigue strength and moderate machinability. While it has better corrosion resistance than the 2000 Al alloys, it may have poorer corrosion resistance than some other aluminum alloys. However, due to its increased cost, its use is limited (la Monaca *et al*., 2021; Siengchin, 2023). To endure the extreme pressure and temperature conditions within the turbine, SS316 sheets were chosen as the material for the annular disc bundle (Srinivasan and Ananth, 2022)(Pineau and Antolovich, 2015). SS316 is a stainless-steel alloy known for its high corrosion resistance, even in harsh settings (Le *et al*., 2018). In some case, aluminum oxide could be considered as the suitable material because they have high corrosion resistance (Abid *et al*., 2023). This substance maintains the discs' durability and lifetime throughout turbine operation.

The shaft, which bears the static stresses, necessitates the use of a material of remarkable strength. EN 24 steel was used for this purpose. EN24 steel is high-tensile alloy steel with excellent wear resistance qualities that are often used in applications requiring high strength and toughness (Khanna *et al*., 2021; Patil *et al*., 2022). It is used for high-strength shafts, gears, connecting rods, punches, and dies in a variety of industries. Table 1 displays the specifics of 7075 Al, SS316, and EN 24, emphasizing their unique qualities pertinent to turbine design. The use of these materials assures the structural integrity of the turbine. The use of these materials maintains the structural integrity, efficiency, and dependability of the turbine under rigorous working circumstances.

2.3 Fabrication and assembly

The bladeless turbine is made up of vital components such as rotating discs, casing, shaft, and nozzle, all of which play important roles in its functioning. The materials for these main components were carefully chosen to fulfill the demanding standards and produce the required turbine performance. To ensure the turbine's best performance and lifetime, materials with exceptional mechanical attributes such as high strength, durability, and corrosion resistance were obtained. Extensive study and testing were carried out to find appropriate materials for each component depending on its unique roles and operating circumstances. To endure the rotating pressures and high temperatures created during operation, the discs, for example, required materials with great tensile strength and heat resistance (Kumar *et al*., 2023; Wang *et al*., 2021). Similarly, materials with high structural integrity and dimensional stability were required for the casing and shaft. After identifying the proper materials, modern machining techniques were used to form the components according to the design parameters. To obtain the needed dimensions, tolerances, and surface finishes, precision machining operations such as turning, milling, and drilling were used (Elsayed and Farghaly, 2022). The use of computer-aided design (CAD) tools, such as SolidWorks, assisted in the generation of precise models and designs, ensuring the technical specifications of the mechanical components were satisfied.

Aside from the primary components, other auxiliary elements were required for the whole turbine system to be

Table 2
Various technical specifications and parameters of Tesla turbine parts

No	Parts	Specifications/Parameters	Dimension
1a	Rotary annular discs	Outer radius (R_o)	24×10^{-3} m
1b		Inner radius (R_i)	2×10^{-3} m
1c		Mean radius (R_m)	13×10^{-3} m
1d		Mean circumference(S)	81.68×10^{-3} m
1e		Thickness (t)	0.35×10^{-3} m
1f		Number of discs (n_d)	15
1g		Spacing between each disc (h)	0.15×10^{-3} m
1h		Number of exhaust holes(n_h)	10
2a	Shaft	Radius (R_i)	2×10^{-3} m
2b		Length (L)	120×10^{-3} m
3	Nozzle	Inlet Area (A)	$75\times 10^{-6} m^2$

assembled. Components such as the pump, coolant supply tank, intercooler, bearings, clamps, bolts, washers, and spacers were supplied. These parts have been collected owing to their tiny sizes or complex patterns from specialized sources having the necessary competence in producing them.

Following theoretical computations and analyses performed with SolidWorks software, a comprehensive table was created to provide an overview of the mechanical component technical specifications and features, as given in **Table 2**. This may be used to assess the critical specifications, parameters, and performance indicators of the turbine's mechanical components while providing a thorough understanding of the design and manufacturing parts. Precision machining methods and careful procurement of auxiliary parts all contribute to the bladeless turbine's successful production. These methods ensure that all of the turbine's components are in functioning order (Balicki *et al*., 2015). Precision machining methods and careful sourcing of auxiliary parts all contribute to the bladeless turbine's successful production. These approaches ensure that the turbine's components are sturdy, trustworthy, and capable of withstanding harsh environments. The combination of theoretical calculations, powerful software analysis, and practical production procedures provides a solid foundation for the turbine's future experimental assessment and validation.

In this part, we go through the significance of each component and its role in the Tesla bladeless turbine. As the driving component, the annular discs effectively replace the usual blades or buckets seen in classic turbines. These discs are organized in a sequence with uniform spacing and are firmly attached to the turbine shaft's middle part. The high-velocity fluid, discharged tangentially from the input nozzle cut in the casing, impinges on the parallel surfaces of the discs. This impinging movement causes the discs to rotate, which causes the turbine shaft to rotate. This bundle of annular discs, as shown in Figure 2a, is designed to resist the whole load during turbine operation, guaranteeing smooth and efficient power output. The diameter of the discs was limited to 50mm due to cost restrictions and an exhaustive academic review. A total of 15 annular discs were made from SS 316 sheets, each having 10 exhaust holes drilled with a vertical milling center machine. Additionally, 0.15mm thick spacers were punched from the same SS 316 sheets. A precision grinding procedure was used to obtain the shaft's surface polish, assuring excellent performance and minimizing friction.

The turbine's overall casing is made up of three separate components. To begin, the center casing, which includes an entrance nozzle, encloses the bundle of annular discs. The hubs on either side, which hold the bearings and accommodate the 10 exhaust holes, are the other two components. All of these components are made of the AL 7075 alloy, which is known for its high strength-to-weight ratio and corrosion resistance. Figure 1b shows how the center casing with the carved intake nozzle was skillfully created utilizing CNC lathe technology. Following the machining process, the housing for the bearing hubs was anodized, as shown in Figure 2c, to increase durability and protect the bearing hubs. Following the machining process, the case for the bearing hubs was anodized, as shown in Figure 2c, to increase durability and protect against environmental influences. We maintain the integrity and performance of the Tesla bladeless turbine by methodically developing and producing these components with the highest accuracy and using appropriate materials. The described components work together to capture the fluid's impinging impact, efficiently converting its energy to rotational motion, and eventually creating power. The mix of high-quality materials, innovative manufacturing processes, and attention to detail in the design process all contribute to the turbine system's overall efficacy and dependability.

3. Assembly and testing of Tesla Turbine

The discs and spacers were mounted onto the shaft of the bladeless turbine during the assembling process. As shown in Figure 3a, this assembly was then firmly fastened within the center shell using bearing hubs and the required bolts and nuts. The turbine assembly, together with other components and a cooling system, was put on a solid wooden test rack to allow testing and assessment, as shown in Figure 3b. The shaft outside the casing was attached to the shaft of a D.C. generator to

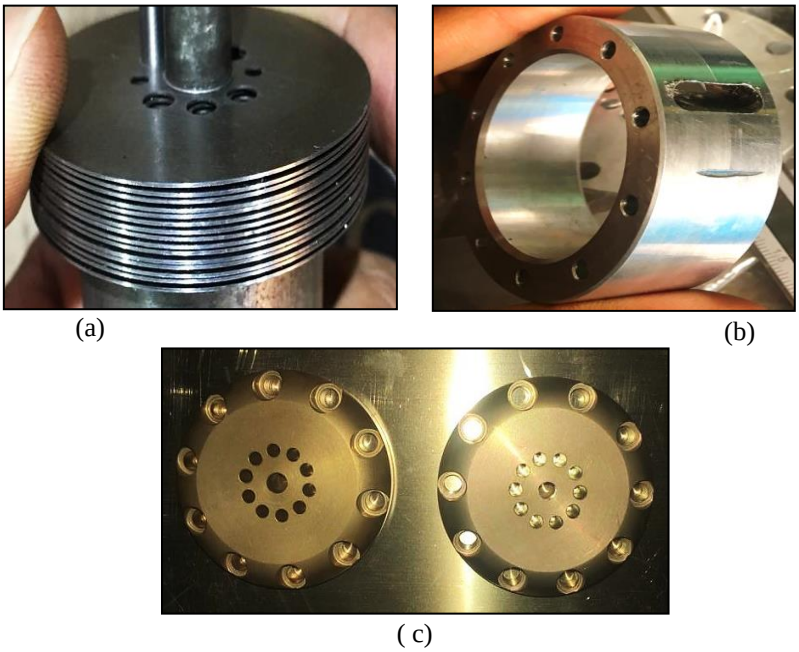

Fig 1. Assembly (a) 48 mm diameter disc assembled; (b) Casing with inlet nozzle; (c) Anodized casing with exhaust holes

(a) (b)

Fig 3. (a) Tesla Turbine Assembly; (b) - Turbine set onto a test rig

capture the mechanical spinning power supplied by the turbine. This connection allowed rotational energy to be transferred from the turbine to the generator. Following the assembling and connection steps, the bladeless turbine was put through a battery of tests using compressed air at various pressures. Several inputs and outputs were methodically measured and computed throughout these test sessions. The major goal was to calculate the electrical power provided by the turbine via the associated generator.

The extensive testing method revealed important information about the turbine's performance and efficiency. Rotational speed, fluid pressure, temperature differentials, and power production were all meticulously monitored and analyzed. The acquired data aided in determining the overall efficacy of the turbine and allowed for further development and optimization of the system. The study team learned a lot about the turbine's operational features and performance by undertaking these exhaustive tests and measurements. The electrical power output was a critical criterion for determining the turbine's ability to generate energy. The test findings were critical in confirming the design ideas, numerical simulations, and manufacturing procedures used during the development process.

4. Results and discussion

4.1 Experimental Results and Discussion

Table 3 provides an in-depth review of the system's performance at various input pressure circumstances that range from 10 to 50 bar. This investigation provides unique insights into the relationship between intake pressure and multiple performance parameters. A key characteristic is the continuous increase in disc angular velocity as incoming pressure increases. The angular velocity at 10 bar is 1130.97 rad/sec, but at 50 bar it soars to 2638.93 rad/sec. This increasing angular velocity indicates the turbine's ability to spin faster when confronted with increased input pressures. This effect is caused by increased fluid momentum and kinetic energy, causing the turbine to spin faster. At the same time, the fluid's exit velocity shows a matching growth pattern. The exit velocity increases from 27.14 m/s to 63.33 m/s as the input pressure increases from 10 to 50 bar. This significant acceleration of the outgoing fluid is linked directly to the turbine's improved performance at greater pressures. The turbine effectively transforms the energy of the fluid that enters into kinetic energy, pushing it at a higher velocity as it departs.

The system's torque increases consistently, rising from 0.0067 Nm at 10 pressures to 0.029 Nm at 50 bar. This expansion is a direct result of the turbine's increasing rotational force at greater input pressures. This higher torque output is due to the increased angular velocity combined with the increased fluid momentum. The system's power output, both thermal and electrical, has risen noticeably. At 10 pressure, the electrical output power surges from 9.52 Watts to 76.52 Watts at 50 bar. This noticeable increase is due to the increased torque and angular velocity at greater pressures. It emphasizes the system's ability to transform mechanical energy into usable electrical power. In contrast, as the inlet pressure rises, so does the input power needed to keep the system running. The input power, which varies from 207.6 Watts at 10 bar to 1069.8 Watts at 50 bar, is proportional to the increased performance levels obtained at higher pressures. The rise in input power reflects the energy required to keep the turbine's speed of rotation and fluid acceleration elevated.

Efficiency, a critical statistic, stays pretty consistent in the 4.58% to 7.15% range. While it varies slightly, it is clear that the system grows more efficient at greater inlet pressures. The turbine's capacity to harness and convert a bigger amount of the incoming fluid's energy into useable mechanical and electrical power contributes to this rise in efficiency. In conclusion, differences in performance measures under different intake pressure levels may be related to the turbine's responsiveness

Table 3
Results during experimental and simulation testing

Inlet Pressure, bar	Experimental/ Simulation	Angular Velocity of Disc, rad/sec	Torque, Nm	Output Power, W	Input Power, W	Efficiency, %	Variation, %
10	Experimental	1130.97	0.0067	9.52	207.6	4.58	16.16
	Simulation	1265	0.0067	9.58	180.07	5.32	
20	Experimental	1507.96	0.011	16.90	323.7	5.22	13.60
	Simulation	1551.25	0.011	16.99	286.51	5.93	
30	Experimental	1884.95	0.018	33.92	581.4	5.83	7.03
	Simulation	2019.58	0.018	34.94	559.63	6.24	
40	Experimental	2261.94	0.022	49.76	773.9	6.43	7.93
	Simulation	2354.25	0.022	53.35	768.76	6.94	
50	Experimental	2638.93	0.029	76.52	1069.8	7.15	10.35
	Simulation	2757.41	0.029	78.57	995.52	7.89	

to changes in fluid momentum, kinetic energy, and flow regimes. Increased intake pressures improve angular velocity, exit speed, torque, and power output, but at the expense of more input power. These findings highlight the turbine's versatility and potential for applications where efficiency optimization is critical, even if increased energy input is required.

4.2 CFD simulation results and discussion

The primary components of the Tesla turbine were designed using a combination of theoretical calculations and SolidWorks software. These calculations and software techniques made it possible to precisely design critical turbine parts. Meshed models of the components were subjected to fluid simulation using ANSYS Computational Fluid Dynamics (CFD) to validate and optimize these designs. The CFD simulations offered important insights into the fluid behavior within the turbine, allowing for design changes to boost its efficiency. Initially, the rotary discs were constructed using technical specifications obtained from theoretical calculations and SolidWorks software. These designs were then used to construct inlet and outlet pieces in ANSYS ICEM software. The component's auto-sized mesh was produced and saved in ICEM format. The meshed model was then imported into the CFD code's pre-processor module, where the necessary boundary conditions for the intake and outflow were implemented. Moving to the CFD code's solver module, the solution was initialized, and the coupled transport equations were solved iteratively until a predefined convergence criterion was met. This method allowed for the precise prediction of fluid flow behavior and turbine performance. Finally, the simulation results were visualized and analyzed in the post-processor module. Flow field parameters such as pressures, velocities, and densities were investigated at various nodes in the flow domain. These findings provided important insights into the turbine's functioning, suggesting places where design changes could improve efficiency as demonstrated by the predecessors (Chen *et al*., 2022, 2021b; Gohil and Saini, 2022; Yadav and Bhagoria, 2013). The predecessors worked on optimized defector design to enhance the performance of wind turbines. The investigators established hydropower instability for small hydro turbines at part load and cavitation erosion at overload operating conditions (Gohil and Saini, 2022). The latter researchers narrowed down the turbulence model for best results in fluid flow and heat transfer simulations (Yadav and Bhagoria, 2013). The redesign of turbine components was facilitated by utilizing the flow field parameters derived by CFD simulation, resulting in increased turbine efficiency and performance optimization.

In the above-mentioned equations, u_r, u_θ, and u_z denotes the components of velocity in radial, azimuthal, and axial directions, correspondingly. p represents pressure, v is the kinematic viscosity, ρ denotes density, T is used for temperature, α denotes thermal diffusivity, and Q is any sink or heat source. These equations, along with appropriate boundary conditions, can be used to simulate the flow through a turbine in cylindrical coordinates.

In this detailed investigation, researchers explore a series of experiments done under varied operational settings to identify the turbine's performance characteristics. Table 3 highlights the core of five unique test scenarios, each aimed at evaluating the turbine's performance under certain parameters marked by nozzle output pressure (Po) and fluid intake velocity. The tests were rigorously carried out to meticulously evaluate numerous crucial performance indicators that provide an in-depth understanding of the Tesla turbine's potential. The angular velocity of the turbine disc is an important performance measure. In the initial test at an exit fluid velocity of 30.63 m/s, an angular velocity of 1265 rad/sec was reached, indicating the turbine's capacity to respond to the starting circumstances. However, what follows is a noteworthy growth. As we progressed through the tests, a steady increase in angular velocity was observed. The Tesla turbine achieved an angular velocity of 2757.41 rad/sec when the exit fluid velocity was 68.57 m/s. This significant rise in angular velocity demonstrates the turbine's capacity to capture energy from high-velocity fluid flows and convert it to mechanical energy. The discharge rate is another critical element under evaluation. This statistic estimates the amount of fluid going through the turbine per unit of time, and its change across the tests is interesting. The initial discharge rate was 0.003 m3/s. However, when the operational conditions altered so did this measure. The discharge rate rose to 7.54 x 1013 m3/s at exit fluid velocity is 68.57 m/s. This significant rise in discharge rate corresponds to the higher fluid velocities and accompanying increases in angular velocity, validating the turbine's ability to handle bigger amounts of fluid successfully. The thermal and electrical output power supplied by the Tesla turbine is crucial. These numbers highlight the practical benefits of its mechanical energy conversion expertise. In the initial test, the turbine produced 10.99 Watts of thermal output power and 9.58 Watts of electrical output power. At higher exit velocities a substantial rise in both thermal and electrical output power was observed. At the peak exit velocity, the thermal output power reached 82.71 Watts, followed closely by electrical output power at 78.57 Watts. These findings highlight the Tesla turbine's potential as an efficient technique of transferring mechanical energy received from fluid flow into thermal and electrical power. Efficiency, which is often viewed as the defining feature of energy conversion machines, needs careful examination. It denotes the percentage of usable output energy to total input energy. The initial test efficiency was 5.32%, indicating space for improvement. Nonetheless, the trajectory is certainly favorable. The efficiency statistic shows steady gains over the tests, with the most recent test having an efficiency of 7.89%. While these efficiency figures are low, they serve as encouraging indicators of the Tesla turbine's improving

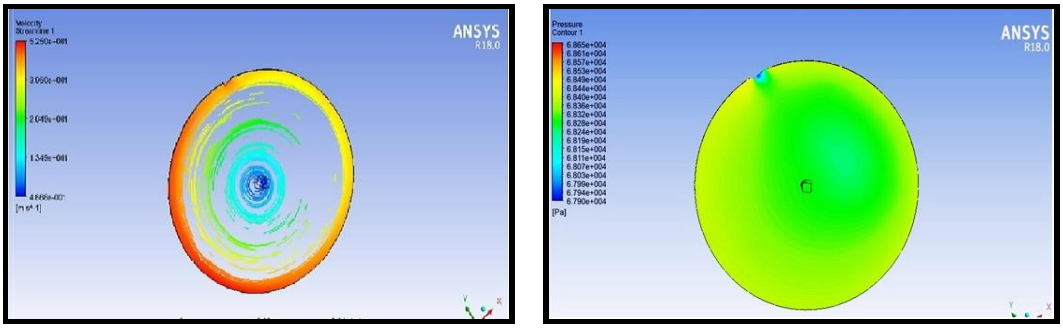

(a) (b)

Fig 4. Contour at 0.6244 bar inlet condition for; (a) Velocity; (b) Pressure

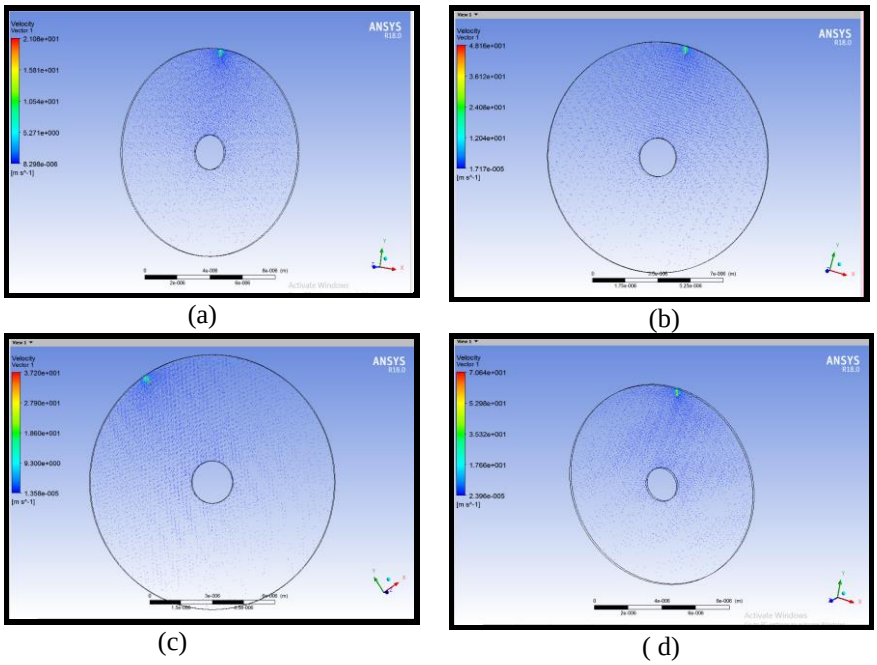

Fig 5. Vector plots at (a) 40; (b) 63; (c) 77; (d) 89 m/s of inlet velocity

ability to transform input energy into meaningful mechanical and electrical power.

The results reveal that the experimental efficiency is 4.58% at 10 bar, whereas the modelling phase efficiency is 5.32%. This suggests that there is a fluctuation of around 16.16% under these conditions. When the input pressure is raised to 20 bar, both the experimental and simulation efficiencies increase, with the experimental reaching 5.22% and the simulation reaching 5.93%. As we increase the input pressure to 30, 40, and 50 bar, this trend persists. Over this range, the simulation consistently outperforms the experimental phase, with variation percentages ranging from 7.03% to 10.35%. To summarize, the data clearly reveals that, given the stated settings, the simulation phase shows higher values ranging from 7.03% to 16.16%.

The flow field parameters at the entry point of the rotating discs are established in this work by studying the nozzle outlet. Figure 4(a) depicts the flow field characteristics contour at 0.6244 bar pressure and 284.07 K temperature, containing air-fluid flowing across the system. The solver module of the CFD code is used to run the simulation, having the flow domain set to rotational. The contour option or the area average of the simulation's velocity may be directly computed to understand the velocity distribution over the whole domain. At discrete sites, various flow field parameters are calculated, allowing the gathering of numerical pressure and temperature measurements. Following this, those outlet values are implemented as the disc's new inlet conditions. The CFD simulation's post-processor module generates numerical values of pressure. The power and efficiency values are calculated

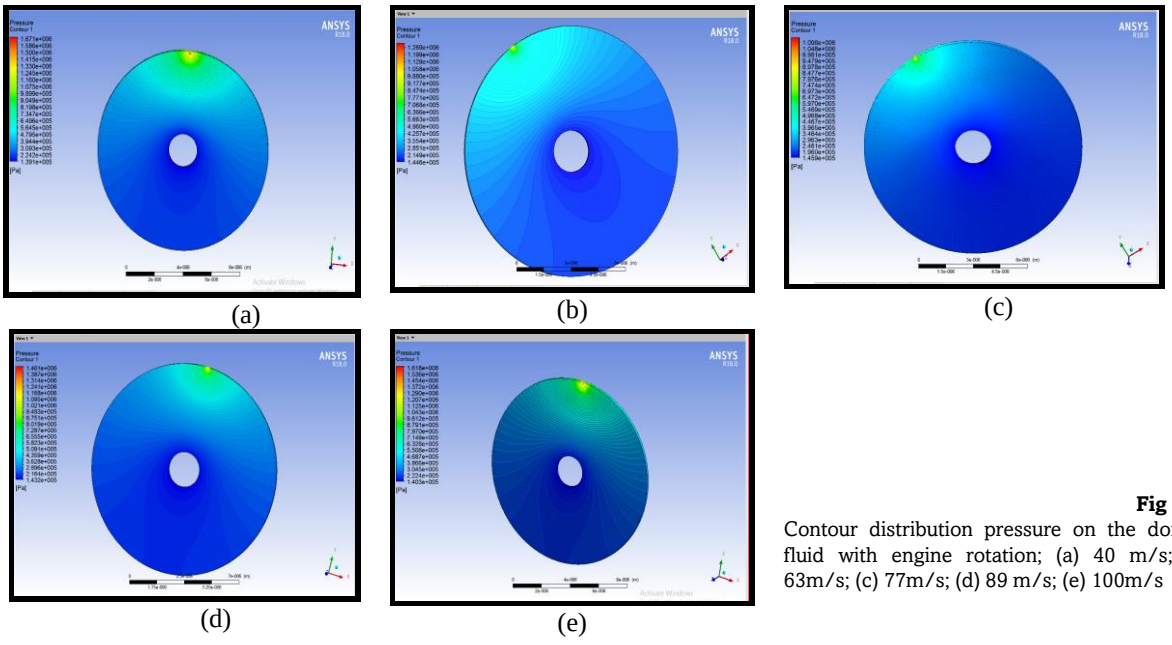

Fig 6. Contour distribution pressure on the domain fluid with engine rotation; (a) 40 m/s; (b); 63m/s; (c) 77m/s; (d) 89 m/s; (e) 100m/s

based on these results. The maximum pressure measured is 0.686 bar, and the minimum pressure measured is 0.679 bar. As illustrated in Figure 4(b), the average pressure throughout the system has been determined to be 0.683 bar.

For higher channel speed cases (40, 63, 77,89, and 100 m/s), there is an observable increase in the surface intensity transition along the range can be found in the power source region. The upsides of the surface intensity transition at the inlet of the nozzle hole in the recreation are lower than in the model as shown in Figure 5(a) vector plot represents the numerical data analytic model. A good agreement between the simulation and the analytic model shows the 40 m/s simulation case. It can be seen in Figure 5(b) that the velocity trend is the same as those shown in Figure 5(c&d). This disparity is related to the unequal speed distribution throughout the recreation's external perimeter and the place from where the data is collected. The tangential speed in the reconstruction was specifically lower than the initial intake speed. The tangential speed is altogether higher than the disc speed. Inside this stream channel, the speeds, as well as the mass and intensity stream, are concentrated and altogether higher than in different districts of the gap. The insightful model can't foresee the improvement of a stream channel and consequently, it neglects to anticipate the ascent of the temperature.

The after-effects of the pressure conveyance in the liquid space of the turbine turn are displayed in Figure 6(a-d). The after-effect of the pressure conveyance in the liquid space shows how the tension contrast acquired in the liquid area depends on the degree colors tracked down in Figure 1 with varieties of 40, 63, 77,89, and 100 m/s. The delta of the Tesla turbines was red. This shows that the best tension exists there. The delta was the initial segment of the stream. The liquid produces an underlying second to drive the plate of the Tesla turbine.

The scientific model can't foresee the improvement of a stream channel and hence, it neglects to anticipate the ascent of the surface intensity motion towards the outlet. In Figure 7, a scalar plot of the temperature dissemination from the analysis is shown. True to form from the surface intensity transition, the temperature at the power source ascends because of the great speeds brought about by the stream channel (Chen *et al*., 2021a).

When numerical simulation results are verified against the physical experimental results, there is good agreement between them both quantitatively and qualitatively, and the average error is 9.79%. From the data of the post-processor module of CFD simulation, all the designed results are computed and compared with the previous results. It was observed that the simulation results have higher quantitative values when compared with the theoretical results based on the physics of the turbine working. The difference in values between such two results for efficiency is illustrated in Figure 5. Such differences creep due to some assumptions and conditions made in the CFD simulation of any components. The outlet-conditioned quantities like the fluid exit velocity, the torque generated, output power, and efficiency vary with the air pressure which runs the turbine.

It was also observed that the electrical power output from the D.C. generator driven by the turbine varies directly with the number of rotary discs in the turbine. In this prototype turbine, 15 rotary discs were used. As per the calculations, the power obtained from each disc adds to the overall power output of the turbine. Hence it was concluded that the more is - the number of rotary discs, the more power can be obtained from the turbine.

5. Conclusions

This study's findings have provided major insights and established a benchmark in understanding fluid flow within annular gaps, establishing their potential for mechanical and electrical power production applications. Bladeless Tesla turbines have far-reaching ramifications in different businesses involved in electrical power generation, notably in serving small communities as well as rural electrification projects, when compared to conventional turbines. Traditional turbines have long worked to reduce losses due to viscosity and the creation of boundary layers. The use of viscous characteristics and boundary layer phenomena in Tesla turbines, on the other hand, provides a revolutionary technique in rotating equipment, with benefits such as decreased or non-existent maintenance costs and simple and economical construction. The goal of this study was to maximize the efficiency of such turbines. Material

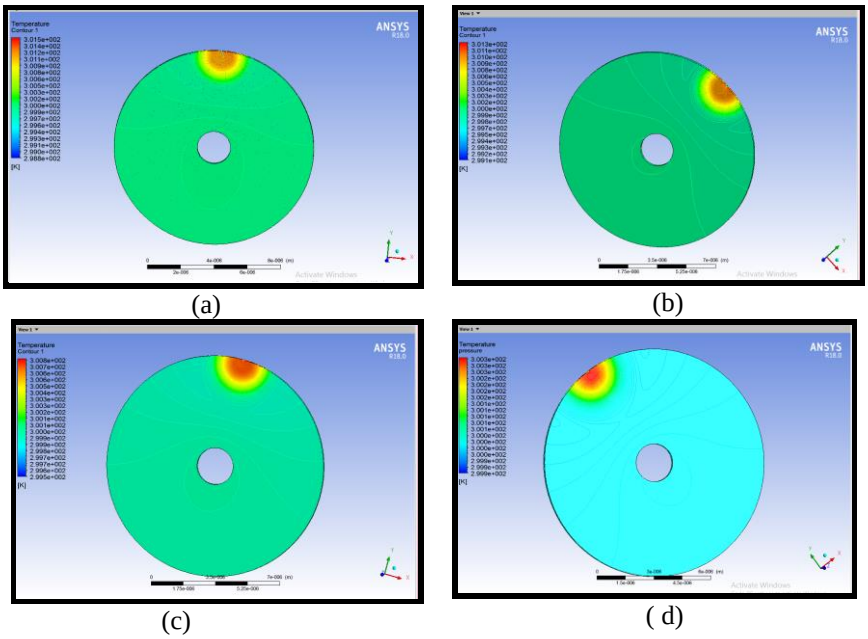

Fig 7. Contour plot at (a) 40; (b) 63; (c) 77; (d) 89 m/s condition for temperature

selection was critical in achieving efficient and sturdy turbine components at a low cost. The casing and intake nozzle was made of 7075 Al, the annular discs were made of SS316, and the shaft was made of EN24 steel. However, there were some limitations to the study. Due to financial constraints and the expensive expense of purchasing 316-grade stainless steel for the discs, the turbine size was limited to a micro-scale or prototype. As a result, the turbine diameter was limited to 48 mm, and the prototype only had 15 discs. It is worth noting that increasing the number of rotational discs increases the power output of the turbine.

Furthermore, the turbine used compressed air as its working fluid, necessitating the usage of an intercooler. Various parts were obtained, and a cooling system was installed to keep the casing cold during turbine operation. Tesla-type rotor discs are noted for their corrosion resistance, making them ideal for rural electrification applications where debris and abrasive two-phase flow are major issues in conventional hydropower generation. However, the low densities of present designs must be considered because they affect the shipping and maintenance of these units, particularly in distant and difficult regions where Pico hydro systems are often put. Tesla turbines offer the potential for Pico hydro applications, but further study is needed to improve their efficiency, reduce fabrication and maintenance costs per kilowatt of power generated, and improve their reliability. Furthermore, investigating the use of wind energy to power Tesla turbines for electricity production could be a fruitful route for future research. Overall, additional R&D efforts are required to improve the efficiency of bladeless turbines and make them more cost-effective for power generation.

Nomenclature

A	Nozzle inlet area, m^2	R_m	Disc mean radius, m
h	Spacing between each disc, m	R_o	Disc outer radius, m
L	The shaft length, m	S	Disc mean circumference, m
max	Maximum	t	Disc thickness, m
n_d	Number of discs	T	Total torque on 'Nd' discs, Nm
n_h	Number of exhaust holes	T_m	Torque at mean radius, Nm
p	Fluid pressure at the inlet, Pa	V_{no}	Exit Velocity of fluid from discs, ms^{-1}
p_{inlet}	Fluid pressure at the nozzle inlet, Pa	V_{isen}	Isentropic flow exit fluid velocity from the nozzle, ms^{-1}
P_T	Total Power from 'nd' discs, W	V_{act}	Actual flow exit fluid velocity from the nozzle, ms^{-1}
P_i	Input Power, W	v	Specific volume, m3 kg-1
P_o	Output Power, W	ρ_{inlet}	Fluid density at the nozzle inlet, kg m-3
Q	Inlet discharge, m^3s^{-1}	ω	Angular Velocity of discs, $rads^{-1}$
R_e	Characteristic Reynolds number	η	Turbine Efficiency
r	Pressure ratio	η_N	Nozzle Efficiency
R_i	Disc inner radius/ or shaft radius, m	γ	Specific heats ratio of gas

References

Abid, M., Kchaou, M., Hoang, A.T., Haboussi, M., 2023. Wear Mechanisms Analysis and Friction Behavior of Anodic Aluminum Oxide Film 5083 under Cyclic Loading. *J. Mater. Eng. Perform*. https://doi.org/10.1007/s11665-023-08616-8

Aghagoli, A., Sorin, M., 2020. CFD modelling and exergy analysis of a heat pump cycle with Tesla turbine using CO2 as a working fluid. *Appl. Therm. Eng*. 178, 115587. https://doi.org/10.1016/j.applthermaleng.2020.115587

Alanne, K., Cao, S., 2019. An overview of the concept and technology of ubiquitous energy. *Appl. Energy* 238, 284–302. https://doi.org/10.1016/j.apenergy.2019.01.100

Alonso, D.H., Silva, E.C.N., 2022. Topology optimization applied to the design of Tesla-type turbine devices. *Appl. Math. Model.* 103, 764–791. https://doi.org/10.1016/j.apm.2021.11.007

Arun, M., Barik, D., Sridhar, K.P., Vignesh, G., 2021. Experimental and CFD analysis of plain and dimples tube at application of solar water heater. *Mater. Today Proc.* 42, 804–809. https://doi.org/10.1016/j.matpr.2020.11.354

Balicki, W., Głowacki, P., Szczeciński, S., Korczewski, Z., Kozakiewicz, A., Szczeciński, J., 2015. Balancing Energy Processes in Turbine Engines. *Polish Marit. Res.* 21, 48–56. https://doi.org/10.2478/pomr-2014-0041

Chen, W.-H., Ocreto, J.B., Wang, J.-S., Hoang, A.T., Liou, J.-H., Hwang, C.-J., Chong, W.T., 2021a. Two-stage optimization of three and four straight-bladed vertical axis wind turbines (SB-VAWT) based on Taguchi approach. e-Prime - Adv. *Electr. Eng. Electron. Energy* 1, 100025. https://doi.org/10.1016/j.prime.2021.100025

Chen, W.-H., Wang, J.-S., Chang, M.-H., Mutuku, J.K., Hoang, A.T., 2021b. Efficiency improvement of a vertical-axis wind turbine using a deflector optimized by Taguchi approach with modified additive method. *Energy Convers. Manag.* 245, 114609. https://doi.org/10.1016/j.enconman.2021.114609

Chen, W.-H., Wang, J.-S., Chang, M.-H., Tuan Hoang, A., Shiung Lam, S., Kwon, E.E., Ashokkumar, V., 2022. Optimization of a vertical axis wind turbine with a deflector under unsteady wind conditions via Taguchi and neural network applications. *Energy Convers. Manag.* 254, 115209. https://doi.org/10.1016/j.enconman.2022.115209

Ciappi, L., Fiaschi, D., Niknam, P.H., Talluri, L., 2019. Computational investigation of the flow inside a Tesla turbine rotor. *Energy* 173, 207–217. https://doi.org/10.1016/j.energy.2019.01.158

Deam, R.T., Lemma, E., Mace, B., Collins, R., 2008. On Scaling Down Turbines to Millimeter Size. *J. Eng. Gas Turbines Power* 130. https://doi.org/10.1115/1.2938516

Dzida, M., Girtler, J., Dzida, S., 2009. On the possible increasing of efficiency of ship power plant with the system combined of marine Diesel engine, gas turbine and steam turbine in case of main engine cooperation with the gas turbine fed in series and the steam turbine. *Polish Marit. Res.* 16, 26–31. https://doi.org/10.2478/v10012-008-0029-1

Elsayed, A.M., Farghaly, M.B., 2022. Theoretical and numerical analysis of vortex bladeless wind turbines. *Wind Eng.* 46, 1408–1426. https://doi.org/10.1177/0309524X221080468

Ernnie Illyani Basri, Adi Azriff Basri, Farah Nur Diyana Salim, 2023. Study on the Effects of Individual Pitot Tube Inlet of a Bladeless Tesla Microturbine using Numerical Analysis. *CFD Lett.* 15, 14–30. https://doi.org/10.37934/cfdl.15.7.1430

Ferrando, M., Caminale, M., Reggio, F., Silvestri, P., 2021. Design and Testing of a Static Rig for Tesla Turbine Flow Visualization, in: Volume 6: Ceramics and Ceramic Composites; Coal, Biomass, Hydrogen, and Alternative Fuels; Microturbines, Turbochargers, and Small Turbomachines. *American Society of Mechanical Engineers*. https://doi.org/10.1115/GT2021-59175

Galindo, Y., Reyes-Nava, J.A., Hernández, Y., Ibáñez, G., Moreira-Acosta, J., Beltrán, A., 2021. Effect of disc spacing and pressure flow on a modifiable Tesla turbine: Experimental and numerical analysis. *Appl. Therm. Eng.* 192, 116792. https://doi.org/10.1016/j.applthermaleng.2021.116792

Gohil, P.P., Saini, R.P., 2022. Investigation into cavitation damage potentiality using pressure pulsation phenomena in a low head Francis turbine for small hydropower schemes. *Ocean Eng.* 263, 112230. https://doi.org/10.1016/j.oceaneng.2022.112230

Guha, A., Smiley, B., 2010. Experiment and analysis for an improved design of the inlet and nozzle in Tesla disc turbines. *Proc. Inst. Mech. Eng. Part A J. Power Energy* 224, 261–277. https://doi.org/10.1243/09576509JPE818

Hassoine, M.A., Lahlou, F., Addaim, A., Madi, A.A., 2022. Improved Evaluation of The Wind Power Potential of a Large Offshore Wind Farm Using Four Analytical Wake Models. *Int. J. Renew.*

Energy Dev. 11, 35–48. https://doi.org/10.14710/ijred.2022.38263
Herrault, F., Yen, B.C., Ji, C.-H., Spakovszky, Z.S., Lang, J.H., Allen, M.G., 2010. Fabrication and Performance of Silicon-Embedded Permanent-Magnet Microgenerators. *J. Microelectromechanical Syst.* 19, 4–13. https://doi.org/10.1109/JMEMS.2009.2036583
Ho-Yan, B.P., 2011. Tesla turbine for pico hydro applications. *Guelph Eng. J.* 4, 1–8.
Hoya, G.P., Guha, A., 2009. The design of a test rig and study of the performance and efficiency of a Tesla disc turbine. *Proc. Inst. Mech. Eng. Part A J. Power Energy* 223, 451–465. https://doi.org/10.1243/09576509JPE664
Huynh, N.D., Lin, Z.-H., Choi, D., 2021. Dynamic balanced hybridization of TENG and EMG via Tesla turbine for effectively harvesting broadband mechanical pressure. *Nano Energy* 85, 105983. https://doi.org/10.1016/j.nanoen.2021.105983
Khanna, N., Agrawal, C., Pimenov, D.Y., Singla, A.K., Machado, A.R., da Silva, L.R.R., Gupta, M.K., Sarikaya, M., Krolczyk, G.M., 2021. Review on design and development of cryogenic machining setups for heat resistant alloys and composites. *J. Manuf. Process.* 68, 398–422. https://doi.org/10.1016/j.jmapro.2021.05.053
Kumar, H., Devade, K., Pratap Singh, D., Mohan Giri, J., Kumar, M., Arun, V., 2023. Severe plastic deformation: A state of art. *Mater. Today Proc.* https://doi.org/10.1016/j.matpr.2023.02.194
la Monaca, A., Murray, J.W., Liao, Z., Speidel, A., Robles-Linares, J.A., Axinte, D.A., Hardy, M.C., Clare, A.T., 2021. Surface integrity in metal machining - Part II: Functional performance. *Int. J. Mach. Tools Manuf.* 164, 103718. https://doi.org/10.1016/j.ijmachtools.2021.103718
Le, T.N., Pham, M.K., Hoang, A.T., Bui, T.N.M., Nguyen, D.N., 2018. Microstructure change for multi-pass welding between Austenitic stainless steel and carbon steel. *J. Mech. Eng. Res. Dev.* 41, 97–102. https://doi.org/10.26480/jmerd.02.2018.97.102
Leaman, A.B., 1950. The Design, Construction and Investigation of a Tesla Turbine. University of Maryland.
LI, Y., GAN, W., ZHOU, W., LI, D., 2023. Review on residual stress and its effects on manufacturing of aluminium alloy structural panels with typical multi-processes. *Chinese J. Aeronaut.* 36, 96–124. https://doi.org/10.1016/j.cja.2022.07.020
Mandaloi, G., Nagargoje, A., Gupta, A.K., Banerjee, G., Shahare, H.Y., Tandon, P., 2022. A Comprehensive Review on Experimental Conditions, Strategies, Performance, and Applications of Incremental Forming for Deformation Machining. *J. Manuf. Sci. Eng.* 144. https://doi.org/10.1115/1.4054683
Manfrida, G., Pacini, L., Talluri, L., 2018. An upgraded Tesla turbine concept for ORC applications. *Energy* 158, 33–40. https://doi.org/10.1016/j.energy.2018.05.181
Manfrida, G., Talluri, L., 2019. Fluid dynamics assessment of the Tesla turbine rotor. *Therm. Sci.* 23, 1–10. https://doi.org/10.2298/TSCI160601170M
Marih, S., Ghomri, L., Bekkouche, B., 2020. Evaluation of the Wind Potential and Optimal Design of a Wind Farm in The Arzew Industrial Zone in Western Algeria. *Int. J. Renew. Energy Dev.* 9, 177–187. https://doi.org/10.14710/ijred.9.2.177-187
Mohammadpour, J., Salehi, F., Sheikholeslami, M., Masoudi, M., Lee, A., 2021. Optimization of nanofluid heat transfer in a microchannel heat sink with multiple synthetic jets based on CFD-DPM and MLA. *Int. J. Therm. Sci.* 167, 107008. https://doi.org/10.1016/j.ijthermalsci.2021.107008
Nguyen, X.P., Le, N.D., Pham, V.V., Huynh, T.T., Dong, V.H., Hoang, A.T., 2021. Mission, challenges, and prospects of renewable energy development in Vietnam. *Energy Sources, Part A Recover. Util. Environ. Eff.* 1–13. https://doi.org/10.1080/15567036.2021.1965264
Pandey, R.J., Pudasaini, S., Dhakal, S., Uprety, R.B., Neopane, D.H.P., 2014. Design and computational analysis of 1 kw Tesla Turbine. *Int. J. Sci. Res. Publ.* 4, 314–318.
Patil, S., Sudhakar Rao, P., Prabhudev, M.S., Yunus Khan, M., Anjaiah, G., 2022. Optimization of cutting parameters during CNC milling of EN24 steel with Tungsten carbide coated inserts: A critical review. *Mater. Today Proc.* 62, 3213–3220. https://doi.org/10.1016/j.matpr.2022.04.217
Peirs, J., Reynaerts, D., Verplaetsen, F., Norman, F., Lefever, S., 2003. Development of a micro gas turbine for electric power generation, in: MME 2003, The 14th MicroMechanics Europe Workshop.
Pineau, A., Antolovich, S.D., 2015. High temperature fatigue: behaviour of three typical classes of structural materials. Mater. High Temp. 32, 298–317. https://doi.org/10.1179/0960340914Z.00000000072
Placco, G.M., Guimarães, L.N.F., 2020. Power Analysis on a 70-mm Rotor Tesla Turbine. J. Energy Resour. Technol. 142. https://doi.org/10.1115/1.4044569
Qi, W., Deng, Q., Chi, Z., Hu, L., Yuan, Q., Feng, Z., 2019. Influence of Disc Tip Geometry on the Aerodynamic Performance and Flow Characteristics of Multichannel Tesla Turbines. Energies 12, 572. https://doi.org/10.3390/en12030572
Qi, W., Deng, Q., Yuan, S., Chen, B., 2023. Advantages of the aerodynamic performance of micro-Tesla turbines. *Energy Sci. Eng.* 11, 1734–1752. https://doi.org/10.1002/ese3.1417
Renuke, A., Vannoni, A., Pascenti, M., Traverso, A., 2019. Experimental and Numerical Investigation of Small-Scale Tesla Turbines. *J. Eng. Gas Turbines Power* 141. https://doi.org/10.1115/1.4044999
Rusin, K., Wróblewski, W., Rulik, S., 2018. The evaluation of numerical methods for determining the efficiency of Tesla turbine operation. *J. Mech. Sci. Technol.* 32, 5711–5721. https://doi.org/10.1007/s12206-018-1118-4
Rusin, K., Wróblewski, W., Strozik, M., 2019. Comparison of methods for the determination of Tesla turbine performance. *J. Theor. Appl. Mech.* 57, 563–575. https://doi.org/10.15632/jtam-pl/109602
Sang, L.Q., Maeda, T., Kamada, Y., Li, Q., 2017. Experiment and Simulation Effects of Cyclic Pitch Control on Performance of Horizontal Axis Wind Turbine. *Int. J. Renew. Energy Dev.* 6, 119–125. https://doi.org/10.14710/ijred.6.2.119-125
Sengupta, S., Guha, A., 2016. Flow of a nanofluid in the microspacing within co-rotating discs of a Tesla turbine. *Appl. Math. Model.* 40, 485–499. https://doi.org/10.1016/j.apm.2015.05.012
Siengchin, S., 2023. A review on lightweight materials for defence applications: Present and future developments. *Def. Technol.* https://doi.org/10.1016/j.dt.2023.02.025
Shoukat, A.A., Noon, A.A., Anwar, M., Ahmed, H.W., Khan, T.I., Koten, H., Siddiqi, M.U.R., Sharif, A., 2021. Blades Optimization for Maximum Power Output of Vertical Axis Wind Turbine. *Int. J. Renew. Energy Dev.* 10, 585–595. https://doi.org/10.14710/ijred.2021.35530
Song, J., Gu, C., Li, X., 2017. Performance estimation of Tesla turbine applied in small scale Organic Rankine Cycle (ORC) system. *Appl. Therm. Eng.* 110, 318–326. https://doi.org/10.1016/j.applthermaleng.2016.08.168
Song, J., Ren, X., Li, X., Gu, C., Zhang, M., 2018. One-dimensional model analysis and performance assessment of Tesla turbine. *Appl. Therm. Eng.* 134, 546–554. https://doi.org/10.1016/j.applthermaleng.2018.02.019
Srinivasan, D., Ananth, K., 2022. Recent Advances in Alloy Development for Metal Additive Manufacturing in Gas Turbine/Aerospace Applications: A Review. *J. Indian Inst. Sci.* 102, 311–349. https://doi.org/10.1007/s41745-022-00290-4
Świrydczuk, J., 2013. Wake-blade interaction in steam turbine stages. *Polish Marit. Res.* 20, 30–40. https://doi.org/10.2478/pomr-2013-0014
Talluri, L., Dumont, O., Manfrida, G., Lemort, V., Fiaschi, D., 2020. Geometry definition and performance assessment of Tesla turbines for ORC. *Energy* 211, 118570. https://doi.org/10.1016/j.energy.2020.118570
Talluri, L., Fiaschi, D., Neri, G., Ciappi, L., 2018. Design and optimization of a Tesla turbine for ORC applications. *Appl. Energy* 226, 300–319. https://doi.org/10.1016/j.apenergy.2018.05.057
Thomazoni, A.L.R., Ermel, C., Schneider, P.S., Vieira, L.W., Hunt, J.D., Ferreira, S.B., Rech, C., Gouvêa, V.S., 2022. Influence of operational parameters on the performance of Tesla turbines: Experimental investigation of a small-scale turbine. *Energy* 261, 125159. https://doi.org/10.1016/j.energy.2022.125159
Wang, X., Gao, X., Zhang, Z., Cheng, L., Ma, H., Yang, W., 2021. Advances in modifications and high-temperature applications of silicon carbide ceramic matrix composites in aerospace: A focused review. *J. Eur. Ceram. Soc.* 41, 4671–4688. https://doi.org/10.1016/j.jeurceramsoc.2021.03.051
Yadav, A.S., Bhagoria, J.L., 2013. Heat transfer and fluid flow analysis of solar air heater: A review of CFD approach. *Renew. Sustain. Energy Rev.* 23, 60–79. https://doi.org/10.1016/j.rser.2013.02.035

Yogesh babu, M.S., Aravind Kumar, S., Hari Prasat, M., Vignesh, R., Devendra Kumar Rao, D., Vijay, A., Reena Christy Elizabeth, S., Jerome Stanley, M., 2020. Design, Fabrication and Analysis of Bladeless Turbine. *IOP Conf. Ser. Mater. Sci. Eng.* 993, 012158. https://doi.org/10.1088/1757-899X/993/1/012158

Zuber, M., Ramesh, A., Bansal, D., 2019. The Tesla Turbine–A Comprehensive Review. *J. Adv. Res. Fluid Mech. Therm. Sci.* 62, 122–137